



Cite this: *Soft Matter*, 2019, 15, 1640

# Continuous assembly of supramolecular polyamine–phosphate networks on surfaces: preparation and permeability properties of nanofilms†

Maximiliano L. Agazzi,<sup>a</sup> Santiago E. Herrera,<sup>a</sup> M. Lorena Cortez,<sup>a</sup> Waldemar A. Marmisollé,<sup>id</sup><sup>a</sup> Catalina von Bilderling,<sup>id</sup><sup>ab</sup> Lia I. Pietrasanta<sup>bc</sup> and Omar Azzaroni<sup>id</sup><sup>\*a</sup>

Supramolecular self-assembly of molecular building blocks represents a powerful “nanoarchitectonic” tool to create new functional materials with molecular-level feature control. Here, we propose a simple method to create tunable phosphate/polyamine-based films on surfaces by successive assembly of poly(allylamine hydrochloride) (PAH)/phosphate anions (Pi) supramolecular networks. The growth of the films showed a great linearity and regularity with the number of steps. The coating thickness can be easily modulated by the bulk concentration of PAH and the deposition cycles. The PAH/Pi networks showed chemical stability between pH 4 and 10. The transport properties of the surface assemblies formed from different deposition cycles were evaluated electrochemically by using different redox probes in aqueous solution. The results revealed that either highly permeable films or efficient anion transport selectivity can be created by simply varying the concentration of PAH. This experimental evidence indicates that this new strategy of supramolecular self-assembly can be useful for the rational construction of single polyelectrolyte nanoarchitectures with multiple functionalities.

Received 23rd November 2018,  
Accepted 8th January 2019

DOI: 10.1039/c8sm02387e

rsc.li/soft-matter-journal

## Introduction

The design of new functional materials based on surface coatings continues to be a great challenge for the scientific and technological community. Ariga and co-workers introduced the concept of “nanoarchitectonics” to describe the development of interfacial multicomponent architectures by the integration of different molecular building blocks in well-defined organized assemblies.<sup>1–7</sup> One of the most powerful strategies used to create multifunctional films is the layer-by-layer (LbL) assembly technique developed by Gero Decher and his collaborators in the early 1990s.<sup>8,9</sup> This technique is based on the step by step adsorption of oppositely charged polyelectrolytes on surfaces which allows the control of structural, compositional and film properties.<sup>10–13</sup> Over the last decades, the frontiers of surface science have been expanded by the appearance of bioinspired

strategies like the spontaneous surface assembly of simple molecules by non-covalent interactions. In this context, Messersmith *et al.* reported and explored a process inspired by dopamine self-polymerization in mussels to build thin films of polydopamine adhered to different surfaces.<sup>14–16</sup> More recently, ultrathin films based on the electrostatic self-assembly of complexes formed by poly(allylamine hydrochloride) (PAH) and phosphate anions (Pi) have been generated and explored for different applications such as redox-active surfaces, electroless metallization, biorecognition, and cell adhesion.<sup>17,18</sup> Supramolecular interactions between polyamines with phosphate anions are present in a significant number of biological and natural processes.<sup>19–24</sup> In previous works, it was demonstrated that the weak polycation poly(allylamine hydrochloride) (PAH) is anionically cross-linked in the presence of single phosphate anions (Pi) forming soft particles of variable size.<sup>25–27</sup> Some reports reveal that these aggregates are stabilized by a combination of electrostatic and hydrogen bonding forces.<sup>28,29</sup>

PAH/Pi films are similar to those obtained by LbL assembly, in the sense that both platforms are constituted by a complex matrix of polyelectrolyte chains. However, in most cases, two polyelectrolytes with opposite charges are required for the traditional LbL assembly and the modulation of the film thickness is mainly attained by changing the number of deposition

<sup>a</sup> Instituto de Investigaciones Físicoquímicas Teóricas y Aplicadas (INIFTA), (UNLP, CONICET), Sucursal 4, Casilla de Correo 16, 1900 La Plata, Argentina. E-mail: azzaroni@inifta.unlp.edu.ar

<sup>b</sup> Departamento de Física, Facultad de Ciencias Exactas y Naturales, Universidad de Buenos Aires, C1428EHA Buenos Aires, Argentina

<sup>c</sup> Instituto de Física de Buenos Aires (IFIBA), (UBA, CONICET), C1428EHA Buenos Aires, Argentina

† Electronic supplementary information (ESI) available. See DOI: 10.1039/c8sm02387e

cycles.<sup>30</sup> In contrast, PAH/Pi platforms generate an ionically cross-linked network from a sole polycation and a single phosphate anion using a one-step technique, by the simple immersion of the substrate in an aqueous solution of the PAH and Pi mixture. In addition, it was observed that the PAH/Pi film thickness can be varied by the concentration of PAH in the mixture, and that its growth is limited for the self-assembly time, reaching a plateau where no more deposition of material is recorded.<sup>17</sup>

In this way, bioinspired assembly of PAH/Pi networks results in a platform based on a single polycation cross-linked supramolecularly. This possibility to build films composed of a single polymer can be useful since the properties of the material are mainly those of the individual polymer, unlike the materials that integrate several macromolecular components.<sup>31,32</sup> One-component cross-linked platforms with modulable thicknesses have previously been reported, however in all the cases, covalent chemistry was required. Generally, single-polymer hydrogels have been built from the LbL assembly of two polyelectrolytes through hydrogen bonding.<sup>33</sup> The polymer of interest was covalently cross-linked and then the other polymer was removed by some specific trigger, such as exposure to basic pH solutions.<sup>34–39</sup> In addition, single polyelectrolyte multilayers have also been designed by the covalent LbL assembly of the same polymer using a covalent cross-linking agent between each deposition step.<sup>40–44</sup>

Herein, we extended the concept of the PAH/Pi assemblies by focusing on the possibility of building tunable phosphate/polyamine-based platforms from specific interactions between multiple PAH/Pi networks deposited in continuous assembly steps. The growth of the films for different deposition steps and the variation in the PAH bulk concentration was analyzed. Besides, the response of the assembly to a specific stimulus such as pH changes was also explored. Lastly, the transport properties of the obtained polymer coatings were electrochemically studied by monitoring the diffusion of redox probes into the film. Experimental data showed that the supramolecular integration of PAH/Pi networks using multiple assembly steps provides a simple strategy to rationally construct single polyelectrolyte nanoarchitectures with interesting controlled properties for multiple applications.

## Experimental

### Chemicals

Polyallylamine hydrochloride (PAH) (*ca.* 58 kDa), cysteamine hydrochloride, (3-aminopropyl)triethoxysilane (APTES), phosphate buffered saline (PBS), ferrocenemethanol (FcOH) and hexammineruthenium(III) chloride were purchased from Sigma-Aldrich. Ethanol, NH<sub>4</sub>OH, NaOH and hydrochloric acid (HCl) were purchased from Anedra. KH<sub>2</sub>PO<sub>4</sub> from Carlo Erba, potassium hexacyanoferrate(III) from Biopack and hydrogen peroxide (100 vol.) from Cicarelli.

The pH values of the stock solutions of Pi (10 mM KH<sub>2</sub>PO<sub>4</sub>) and PAH (1 mg mL<sup>-1</sup>) were adjusted to 7 by adding 10% NaOH. Also, the Pi solutions were adjusted to basic pH with 10%

NaOH. Acid solutions of Pi were adjusted with aqueous HCl solution (10 mM). All chemicals were of analytical grade. Water used in all experiments was purified using a Millipore system and its resistivity was 18.2 MΩ cm.

### PAH/Pi-coated substrate preparation

PAH/Pi-coated substrates were fabricated from stock solutions of PAH and Pi (KH<sub>2</sub>PO<sub>4</sub>), both at pH = 7. The substrate was placed vertically in the interior of the cell and equal volumes of PAH (0.1 and 0.4 mg mL<sup>-1</sup>) and Pi solutions (10 mM) were added. After 15 minutes of deposition, the substrate was rinsed with Pi (10 mM) for another 5 minutes. This process was repeated to obtain PAH/Pi films with different assembly steps.

Gold-sputtered glass slides modified with cysteamine were used as substrates for surface plasmon resonance and electrochemical experiments. APTES-modified Si slides were used as substrates for AFM measurements. For cysteamine modification, Au substrates were typically soaked overnight in a 2 mM cysteamine ethanolic solution. Then, substrates were thoroughly rinsed with ethanol and water, and dried under a stream of nitrogen gas.

Si substrates were incubated in an ethanolic solution of 2% APTES for 1 h, rinsed with ethanol and annealed for 2 h at 120 °C.

### Surface plasmon resonance

SPR detection was carried out using a SPR-Navi 210A setup (BioNavis Ltd, Tampere, Finland). SPR gold sensors were cleaned by immersing them in boiling NH<sub>4</sub>OH (28%)/H<sub>2</sub>O<sub>2</sub> (100 vol) 1:1 for 15 min and then rinsing with water and ethanol. Then, they were modified with cysteamine. An electrochemistry flow cell (SPR321-EC, BioNavis Ltd) was employed for all measurements. The injection was performed manually and SPR angular scans (two wavelength mode) were recorded with no flow in the cell. The temperature was kept at 20 °C. All SPR experiments were processed using the BioNavis Data viewer software.

### Atomic force microscopy

Si substrates modified with APTES and coated with (PAH/Pi)<sub>*n*</sub>, where *n* is the number of deposition cycles (*n* = 1, 4, 7 and 10), were analyzed *via* Atomic Force Microscopy (AFM). A Bruker Multimode atomic force microscope connected to a Nanoscope V controller was used to image the topography of the substrate. AFM tapping mode measurements were performed under dry nitrogen ambient, using RTESP (Bruker, *K* = 40 N m<sup>-1</sup>) cantilevers. Images were processed by flattening using the NanoScope software to remove the background slope. The roughness RMS value of each image was obtained using the NanoScope software.

For the thickness measurement, AFM scanning was first performed in a contact mode at high forces, removing all polymer to expose bare silicon. Sectional analysis of several profiles from a subsequent zoomed out tapping mode scan was used to evaluate the thickness.

### Size and zeta potential measurements

The size of PAH/Pi complexes was determined by Dynamic Light Scattering (DLS) employing a Zetasizer Nano system (Nano ZSizer-ZEN3600, Malvern, U.K.) at 25 °C employing a distribution fitting method. The zeta potential was determined from the electrophoretic mobility measured by Laser Doppler Velocimetry using a Zetasizer Nano system. Measurements were performed using disposable capillary cells (DTS 1061 1070, Malvern) at 25 °C with a drive cell voltage of 30 V and employing the monomodal analysis method.

### Electrochemical measurements

Cyclic voltammetry experiments were performed using a Gamry REF600 potentiostat and a conventional three-electrode cell equipped with an Ag/AgCl (3 M KCl) reference electrode and a platinum counter electrode. Cyclic voltammograms of  $\text{Fe}(\text{CN})_6^{4-}$ ,  $\text{Ru}(\text{NH}_3)_6^{3+}$  and FcOH in Phosphate Buffered Saline (PBS: 10 mM Pi, 2.7 mM KCl, 137 mM NaCl, pH 7.4) were registered on Au/cysteamine (Au/cys) substrates modified with  $(\text{PAH}/\text{Pi})_n$  assemblies ( $n = 0, 1, 2, 3, 4$  and 5). Cyclic voltammograms presented are those obtained in the third cycle of a total of five consecutive cycles of the potential. The peak current showed a very high stability with the number of cycles, with which the deviation standard between each magnitude was negligible.

## Results and discussion

The construction of multiple PAH/Pi networks in solid substrates was conducted through successive deposition steps (Fig. 1). The formation of the films was monitored using SPR measurements. Au sensors were first chemically modified with cysteamine to confer a net positive charge to the substrate. PAH and Pi solutions at pH 7 were mixed and immediately injected to the SPR cell. After 15 minutes of deposition, the substrate was rinsed with Pi solution for another 5 minutes. This methodology was repeated for each new assembly step. The growth of the films was monitored for different concentrations of PAH (0.01, 0.025, 0.05, 0.1 and 0.2  $\text{mg mL}^{-1}$ ) in 5 mM Pi.

Fig. 2 shows the evolution of the angle of minimum reflectivity of the Au-cys modified SPR sensors during the assembly of the PAH/Pi networks for ten injection cycles. The obtained sensograms indicate that the films based on multilayers of PAH/Pi networks grow effectively and the deposited material remains stable after each washing step. This stability indicates that this supramolecular architecture is sustained by specific interactions between the PAH chains and phosphate anions. This continuous growth suggests that after each assembly cycle, some amine groups and phosphate anions in the deposited network remain free to interact through electrostatic interactions and hydrogen bonding with the new PAH/Pi complexes, which become integrated in the next cycle (Fig. 1C). Hydrogen-bond interactions between amino groups and phosphate anions have widely been recognized in a variety of supramolecular systems. On one side, they have been postulated to be responsible for the tridimensional stabilization of the nuclear aggregates of polyamines.<sup>45</sup> On the other hand, Kooijman and co-workers have also shown that the hydrogen bond interaction between amine groups of proteins and phospholipids induces further dissociation degree of phosphate moieties, increasing the protein binding interaction on the lipidic membranes.<sup>46</sup>

The presence of hydrogen bonding between ammonium groups and phosphate anions has also been employed for explaining the specific binding of phosphates on amino-modified surfaces.<sup>47</sup> The relative importance of this interaction has been used to justify the much higher affinity for phosphate species as compared to other anions.

Moreover, the importance of hydrogen-bond interactions has extensively been recognized in the formation of aggregates between polyamines and phosphates,<sup>48</sup> as this type of interaction favors the formation of tridimensional networks.<sup>49</sup> In this case, the possibility of setting a hydrogen bond network seems to be essential as an orthophosphate anion meets both the structural geometric requirements and the ability to form hydrogen bonds. It has been shown that the phosphate anion forms aggregates with PAH more efficiently than other divalent anions and this has suggested the possibility of additional

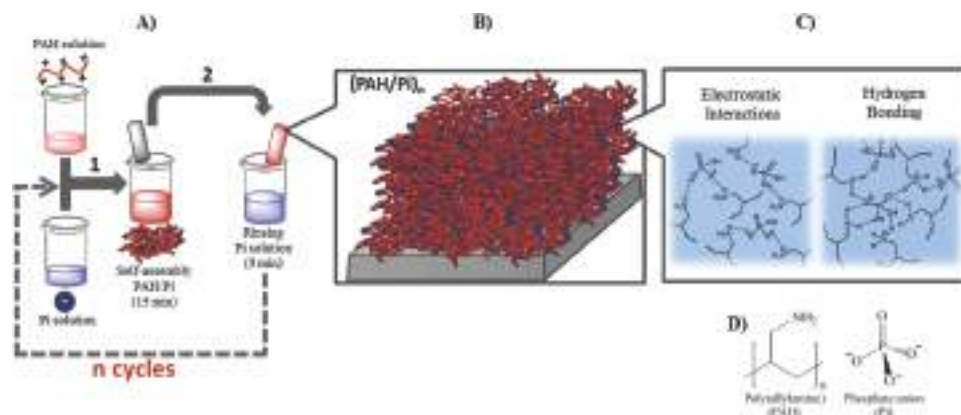


Fig. 1 (A) Representation of the assembly procedure for surface modification with polyamines and phosphate ions, (B) simplified representation of PAH/Pi networks after  $n$  cycles of assembly, (C) the interaction mechanism between PAH and Pi species and (D) chemical structures of PAH and Pi.

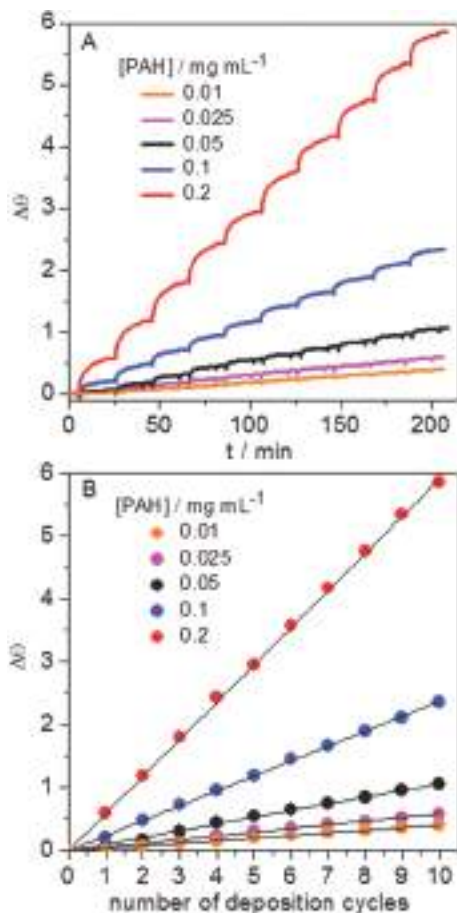


Fig. 2 (A) Change in the minimum reflectivity angle ( $\Delta\theta$ ) of the SPR scan (measured at  $\lambda = 785$  nm) during the formation of multilayered PAH/Pi coatings on cysteamine-modified Au substrates from PAH solutions of different concentrations in 5 mM pH 7 Pi buffer. (B) Dependence of the  $\Delta\theta$  plateau on the number of deposition cycles.

proton dissociation induced by interaction with protonated amines of PAH.<sup>50</sup>

The formation of hydrogen bonding has also been argued to be responsible for the high and specific association between phosphate anions and amine groups of PAH-modified silica microparticles,<sup>51</sup> where the remarkable surface charge reversion cannot be explained by electrostatic interactions only.

Furthermore, FTIR studies of PAH/Pi coatings indicate that phosphate groups are not connected as in the case of crystalline solids such as  $\text{KH}_2\text{PO}_4$  and  $\text{NH}_4\text{H}_2\text{PO}_4$ , but they are in a more amorphous environment, consistent with those structures depicted in Fig. 1C. The same features have been reported for amorphous  $\text{NH}_4\text{H}_2\text{PO}_4$  where the formation of hydrogen bonds between the ammonium and  $\text{H}_2\text{PO}_4^-$  groups has been proved.<sup>52</sup>

Besides the growth mechanism, Fig. 2A clearly shows that the amount of material deposited increases with the PAH concentration. In addition, it is observed that the deposition rate decreases with time over each deposition cycle, until reaching a plateau. However, the time required for reaching that plateau is less for lower PAH concentrations. In addition, Fig. 2B shows that changes in the minimum reflectivity angle ( $\Delta\theta$ )

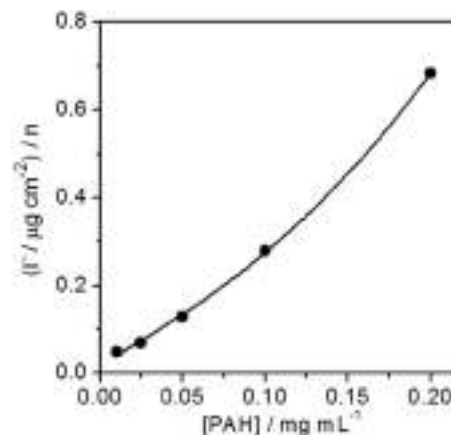


Fig. 3 Dependence of surface coverage for the deposition cycle on initial PAH bulk concentration.

depend linearly on the number of deposition cycles, evidencing a notoriously regular growth under all the assembly conditions evaluated.

The surface coverage of the PAH/Pi complexes for each assembly cycle was estimated from SPR measurements for the different concentrations of PAH (Fig. 3). The calculation was carried out using the angle change, sensitivity factors of the SPR and  $dn/dc = 0.16 \text{ cm}^3 \text{ g}^{-1}$  for PAH solutions.<sup>53</sup> These results indicate that the amount of deposited material increases exponentially with the polyelectrolyte concentration.

PAH/Pi films were characterized by atomic force microscopy. For this purpose, equivalent volumes of PAH (0.4 and 0.1 mg mL<sup>-1</sup>) and Pi (10 mM) solutions, both at pH 7, were mixed in a cell containing a flat silicon substrate modified with APTES. The material was deposited over the surface with the assembly methodology presented in Fig. 1. AFM topographic imaging was performed on (PAH/Pi)<sub>n</sub> films formed by different deposition cycles ( $n$ : 1, 4, 7 and 10). Fig. 4 shows AFM imaging of PAH/Pi-coatings assembled from 0.2 mg mL<sup>-1</sup> PAH in 5 mM Pi pH 7. The surface topography indicated that PAH/Pi complexes are evenly distributed on the substrate generating a fairly homogeneous coating after the assembly process. In addition, images reveal the presence of important protuberances that increase in their amount and height with the deposition cycles. It was also observed that the surface roughness increases markedly with the number of deposition cycles. The RMS roughness of the PAH/Pi coatings can be estimated to be 5, 66, 85, and 95 nm for samples prepared from 1, 4, 7 and 10 cycles, respectively. Similar topographic features were observed for PAH/Pi films formed from 0.05 mg mL<sup>-1</sup> PAH in 5 mM Pi pH 7 (Fig. S1, ESI†).

In addition, the coating thickness of the film formed from 0.05 mg mL<sup>-1</sup> PAH with a single deposition cycle (PAH/Pi)<sub>1</sub> was measured *via* AFM. For this purpose, scanning was performed in a contact mode under harsh conditions (high forces), removing all polymer and exposing bare silicon (Fig. S2, ESI†). From this “effective” thickness ( $\sim 2.4$  nm), the refractive index of the material was estimated by adjusting the experimental SPR curves with the “Winspall” software. Using the refractive

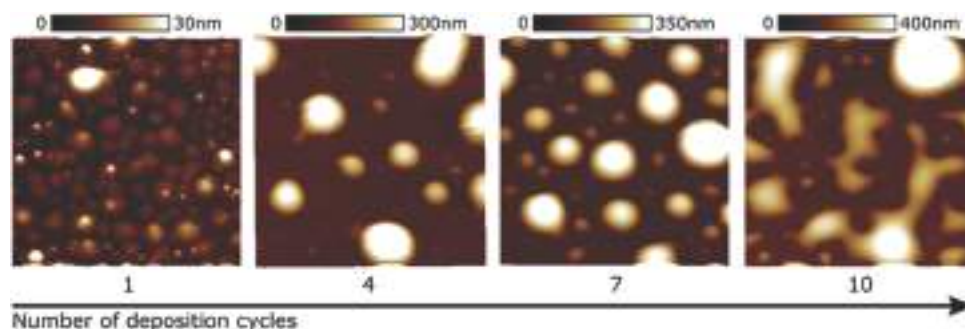


Fig. 4 AFM height images of  $(\text{PAH}/\text{Pi})_n$  for  $n = 1$  (RMS roughness: 5 nm), 4 (RMS roughness: 66 nm), 7 (RMS roughness: 85 nm) and 10 (RMS roughness: 95 nm). Imaging was performed in a tapping mode, in dry nitrogen ambient. Z scales are indicated on each image, with a scan size of  $5 \mu\text{m}^2$ .

index obtained ( $n = 1.40$ ), thickness values were estimated for the subsequent assembly cycles and for films with different PAH bulk concentrations (Fig. 5). The results show that this soft-assembly strategy of PAH/Pi networks allows to create films with nanometer-scale thickness control.

So far, the results obtained allow us to infer that it is possible to construct a platform of modulable thickness based on a single ionically cross-linked macromolecular component. It is interesting to note that our approach allows us to build under mild conditions, single polymer matrices of different thicknesses based entirely on supramolecular interactions between the PAH/Pi networks generated in each assembly cycle. In a previous study, we explored a wide spectrum of functionalities for PAH/Pi films generated by a one-step self-assembly.<sup>17</sup> For example, simple derivatization of pendant amino groups of PAH precursors with hydroquinone and biotin provided an efficient electrochemical response and biorecognition capacity, respectively. Thus, the possibility of modulating the film thickness would allow expanding and optimizing the functionalities through a controlled and hierarchical organization of functional domains.

Subsequently, in order to improve our understanding of the interfacial assembly process, we studied the formation of PAH/Pi complexes in solution under the same experimental conditions as those of the SPR studies. Fig. 6A shows the time

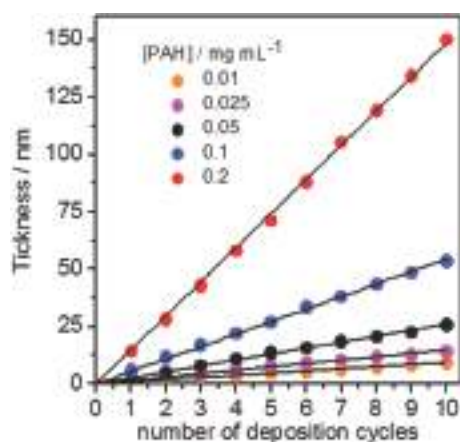


Fig. 5 Thickness evolution of PAH/Pi films as a function of the number of deposited layers at different PAH bulk concentrations.

evolution of the hydrodynamic diameter of PAH/Pi aggregates in the solution phase, formed by adding PAH solutions (final concentrations: 0.01, 0.025, 0.05, 0.1 and 0.2  $\text{mg mL}^{-1}$ ) to a 5 mM pH 7 Pi solution. PAH/Pi colloids showed a dynamic behavior with initial sizes between 150 and 300 nm. However, when the PAH concentration was  $\leq 0.1 \text{ mg mL}^{-1}$ , a noticeable increase in the size as a function of time was observed. This is due to the coagulation of the PAH/Pi colloids and the consequent formation of larger aggregates. Nevertheless, size growth is much lower in colloids formed at the highest concentration of PAH (0.2  $\text{mg mL}^{-1}$ ), showing higher stability over time. Very recently, Andreozzi *et al.* reported a similar behavior in other PAH/Pi colloids.<sup>54</sup> It is important to emphasize that the magnitude of the hydrodynamic diameters of the PAH/Pi aggregates is much higher than the corresponding thicknesses of the films. This could indicate that the interfacial assembly is constructed mainly by the deposition of the first PAH/Pi networks complexed in solution and that the larger aggregates observed by DLS constitute the protuberances that are observed in the AFM images.

Fig. 6B shows the values of the zeta potential obtained for each solution phase sample. It is known that the cross-linking of the polymer chains by the anion decreases the overall positive charge of the polyamine chains.<sup>55</sup> We observed that the zeta potential increases with the PAH concentration from an almost neutral potential for 0.01  $\text{mg mL}^{-1}$  up to a positive value of around 20 mV for 0.2  $\text{mg mL}^{-1}$ . At higher concentrations of PAH the cross-linker/polycation ratio decreases in the complexes, and the charge compensation in the polymer chains is lower. Besides, these results indicate that the growth mechanism is charge-limited. Thus, size growth can be explained by considering a balance between electrostatic repulsions and van der Waals attractions.<sup>56</sup> A higher zeta potential makes the size smaller due to the electrostatic repulsion between the complexes, while small zeta potential decreases the repulsion, and causes rapid growth and greater coagulation.

The time dependence of the scattered intensity is shown in Fig. 6C as obtained from the derived count rate of each measurement, expressed as kilocounts (kcounts). The scattered intensity depends on the diameter of the aggregates and their concentration in solution. The derived count rate decreases with time in all the cases due to the coagulation and precipitation of the PAH/Pi aggregates, but for 0.2  $\text{mg mL}^{-1}$  of PAH this

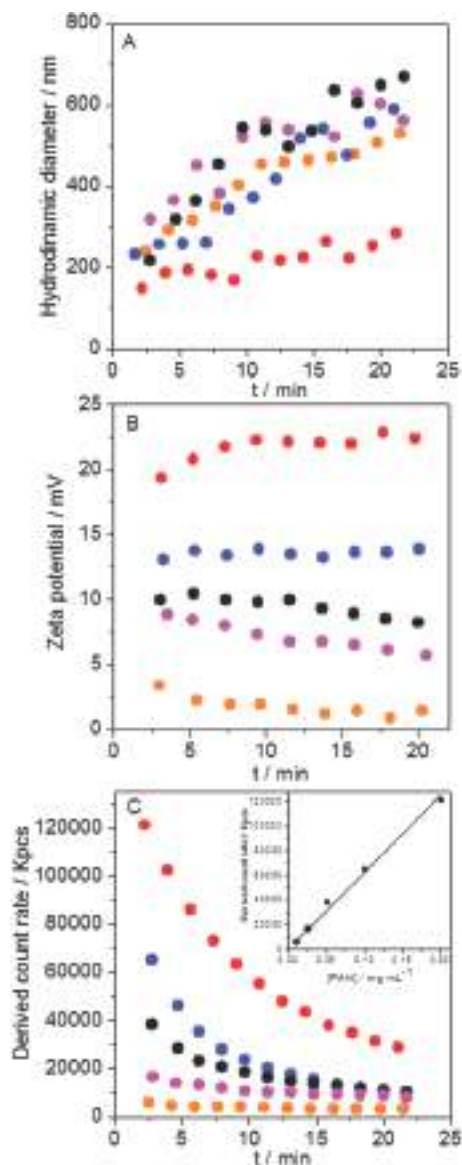


Fig. 6 Time dependence of size (A), zeta-potential (B) and the derived count rate (C) of PAH/Pi colloids at the five concentrations of [PAH]: 0.2 mg mL<sup>-1</sup> (red circles), 0.1 mg mL<sup>-1</sup> (blue circles), 0.05 mg mL<sup>-1</sup> (black circles), 0.025 mg mL<sup>-1</sup> (pink circles) and 0.01 mg mL<sup>-1</sup> (orange circles) in 5 mM pH 7 Pi buffer. Inset in (C): the initial derived count rate for each concentration of PAH.

decrease is lower. The inset of Fig. 6C shows the variation of kcounts with the initial time as a function of PAH concentration. It is observed that the kcounts increases clearly with the concentration of the polyelectrolyte, probably revealing that the concentration of the PAH/Pi complex formed initially increases with the amount of PAH added. This explains that at a higher concentration of added PAH, more material is deposited on the substrate surface. In addition, the higher temporal stability of complexes formed from 0.2 mg mL<sup>-1</sup> PAH may also contribute to more extended deposition processes, since the lower precipitation of aggregates allows extending the period of surface assembly. This is reflected in the sensograms of Fig. 2A, where

it is observed that the angle of growth does not reach a well-marked plateau after 15 minutes of deposition, as observed in other PAH concentrations.

### Film stability

The stability of the films under different pH conditions was evaluated by SPR. In many applications, it is important that functional polymeric films can be disassembled by a specific stimulus.<sup>57</sup> PAH is a weak polycation (effective  $pK_a = 8.5$ )<sup>58</sup> and the phosphate ion participates in three acid/base equilibria with  $pK_{a1} = 2.12$  ( $H_3PO_4/H_2PO_4^-$ ),  $pK_{a2} = 7.20$  ( $H_2PO_4^-/HPO_4^{2-}$ ) and  $pK_{a3} = 12.36$  ( $HPO_4^{2-}/PO_4^{3-}$ ).<sup>59</sup> As the ionization degrees of PAH and Pi vary with pH, PAH/Pi films may be dissolved by pH changes. The stability with the pH of the PAH/Pi coating formed by a single deposition cycle was previously evaluated using a quartz crystal microbalance, observing that PAH/Pi monolayers remain stable up to pH 3 and dissolve completely at pH 12.<sup>17</sup> In this sense, the pH-response of the multilayers of PAH/Pi networks was evaluated by SPR injecting Pi solutions at different pH values. We observed that the films formed from 0.05 mg mL<sup>-1</sup> PAH in 5 mM Pi were stable up to pH 4 presenting a small increase of the minimum angle, possibly due to the greater protonation of PAH that requires binding of more anions for charge compensation (Fig. 7A). However, at pH 3.5 the supramolecular platform starts dissolving, being

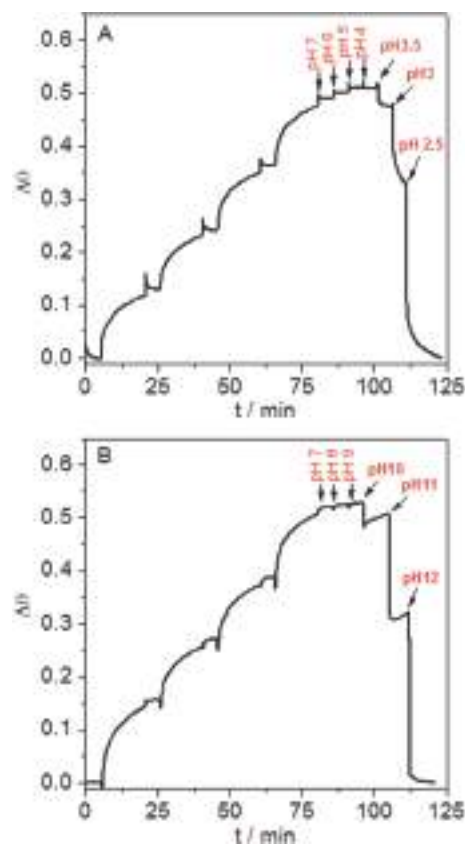


Fig. 7 Change in the minimum reflectivity angle of the SPR scan (measured at  $\lambda = 785$  nm) for the (PAH/Pi)<sub>4</sub> coatings (0.05 mg mL<sup>-1</sup> PAH/5 mM Pi) during the injection of Pi solutions at acidic pH (A) and basic pH (B).

completely removed at pH 2.5. At this low pH, the protonation of the Pi ions facilitates the disassembly by the removal of the stabilizing electrostatic interactions between the PAH chains and the cross-linker ions. At basic pH, the polymer network remains assembled up to pH 10 and it is completely removed at pH 12 (Fig. 7B). Under these conditions, PAH amine groups are deprotonated causing the dissolution of the ionic network. A similar pH response was reported for macroscopic gels formed by PAH chains cross-linked by polyphosphates such as pyrophosphate anions (PPi) and tripolyphosphate (TPP).<sup>60,61</sup>

Coatings formed from  $0.2 \text{ mg mL}^{-1}$  PAH and  $5 \text{ mM}$  Pi show a small difference in stability in contact with acid solutions, since they are dissolved below pH 4 and completely removed at pH 3 (Fig. S3, ESI†). This behavior may be due to the assembly being produced from a lower PAH/Pi ratio. Thus, the supra-molecular networks present a lower ionic crosslink density, generating a matrix that is more unstable to the protonation of the phosphate groups.

### Film permeability

Finally, the permeability of PAH/Pi films with different assembly steps and at two bulk concentrations of PAH was analyzed. The evaluation of the transport properties of the interfacial

nanoarchitectures is relevant not only to explore their structural characteristics but also to guide the study of the materials towards certain practical applications such as membrane-based separations, filtration systems, sensors, bioactive release systems and biologically active coatings.<sup>62–67</sup> Different efforts have been made to design nanoarchitectures with suitable transport properties. In this context, the permeability properties of LbL assemblies with the aim of creating smart ion separation membranes have been studied.<sup>68,69</sup> However, for most polyelectrolyte films the ion permeability is relatively poor, due to the intrinsic charge compensation between the constituent polyelectrolytes. The ion-selectivity modulation of multilayer films was generally explored by controlling the surface charges of the assemblies.<sup>70,71</sup> Also, weak polyelectrolyte multilayers prepared by the LbL assembly and covalently stabilized with a cross-linking agent showed ion permselectivity with pH changes.<sup>72,73</sup> In addition, several methods that insert a net charge and nanoporosity into films have been developed to construct ionic permselectivity membranes.<sup>74,75</sup>

We explored the permeability of our coatings by analyzing the electrochemical response of a film-coated electrode *via* cyclic voltammetry (CV) in the presence of hexacyanoferrate ( $\text{Fe}(\text{CN})_6^{3-}$ ) (negative probe), hexaaminoruthenium ( $\text{Ru}(\text{NH}_3)_6^{3+}$ )

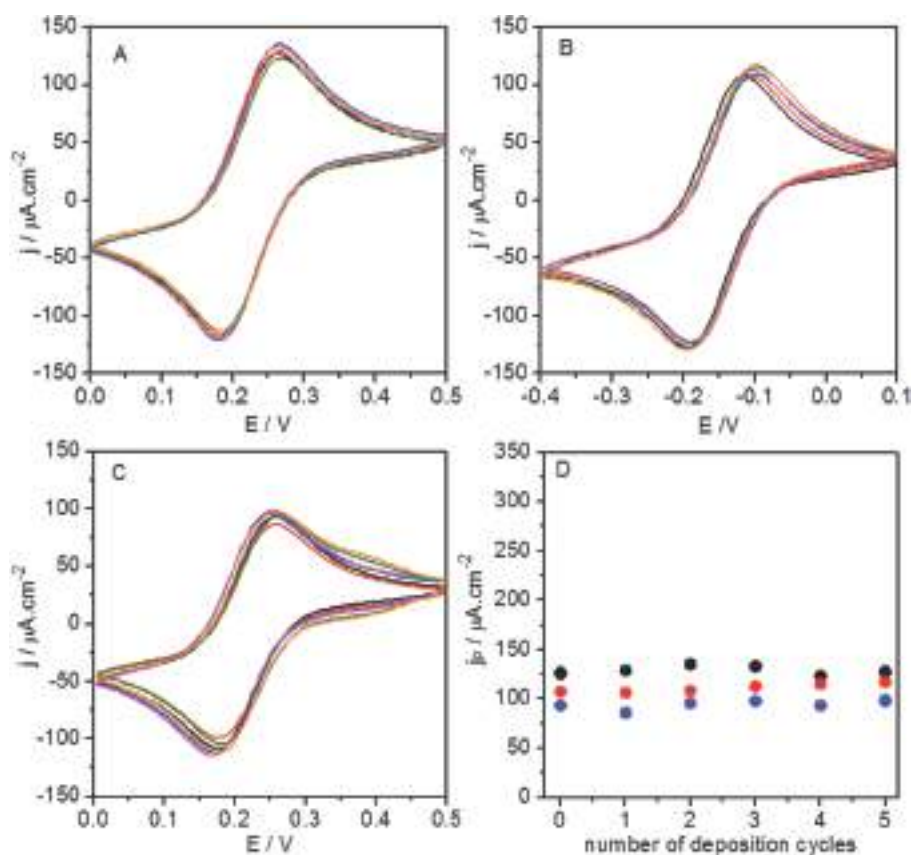


**Fig. 8** Cyclic voltammograms of Au/cys (black lines) and Au/cys modified with PAH/Pi films formed from  $0.05 \text{ mg mL}^{-1}$  PAH in  $5 \text{ mM}$  Pi pH 7, with different number of deposition cycles: (PAH/Pi)<sub>1</sub> (red lines), (PAH/Pi)<sub>2</sub> (blue lines), (PAH/Pi)<sub>3</sub> (pink lines), (PAH/Pi)<sub>4</sub> (green lines) and (PAH/Pi)<sub>5</sub> (orange lines), in PBS buffer containing  $1 \text{ mM}$  of (A) FcOH, (B)  $\text{Ru}(\text{NH}_3)_6^{3+}$  and (C)  $\text{Fe}(\text{CN})_6^{4-}$ . (D) Anodic peak current density ( $j_p$ ) as a function of the number of deposition cycles for FcOH (black circles),  $\text{Ru}(\text{NH}_3)_6^{3+}$  (red circles) and  $\text{Fe}(\text{CN})_6^{4-}$  (blue circles). Error bars are smaller than the symbol size. Scan rate:  $0.050 \text{ V s}^{-1}$ .

(positive probe) and ferrocene methanol (FcOH) (neutral probe) aqueous solutions. These redox probes have comparable sizes, so it is expected that permeation is influenced mainly by the charge of each species.<sup>76</sup> Electrochemical experiments were performed with 1 mM of each redox probe in PBS as a supporting electrolyte. It should be noted that this medium with a high saline concentration did not affect the structural integrity of the self-assembled film (Fig. S4, ESI†).

Fig. 8 describes the CVs of films assembled from 0.05 mg mL<sup>-1</sup> PAH in 5 mM Pi pH 7, in PBS solution containing FcOH (A), Ru(NH<sub>3</sub>)<sub>6</sub><sup>3+</sup> (B) and Fe(CN)<sub>6</sub><sup>3-</sup> (C). For comparison, the electrochemical response of the redox probes on the unmodified Au-cys electrode (black lines) is also shown. It can clearly be seen that the magnitude of the voltammetric signal, which reflects the transport of electroactive probes towards the underlying conductive support, is not affected by the presence of PAH/Pi networks with different thicknesses. The current density of the anodic peak as a function of the number of PAH/Pi deposition cycles, as shown in Fig. 8D, reveals that the permeability of the three redox species does not change markedly with the number of assembly steps. In addition, no relevant changes

are observed in the position of the redox potential, and the separation between anodic and cathodic peaks remains constant for each redox couple. This indicates that the kinetics of electron and mass transfer processes do not change with the thickness of the film regardless of the net charge of the redox probes.

On the other hand, clear differences were observed when studying the permeation of the films formed by mixing 0.2 mg mL<sup>-1</sup> PAH in 5 mM Pi pH 7 (Fig. 9). In the case of Ru(NH<sub>3</sub>)<sub>6</sub><sup>3+</sup>, the permeability decreases markedly from complete permeation for (PAH/Pi)<sub>1</sub>, to a practically complete suppression of the redox response for (PAH/Pi)<sub>5</sub> (Fig. 9B). However, the voltammetric response in the presence of neutral FcOH shows no differences for the different coating thicknesses, as observed for films formed from 0.05 mg mL<sup>-1</sup> PAH solutions. These results indicate that the permeation properties of the neutral probe are not affected by the amount of the material deposited and, thus, the hindrance observed for the positive probe is not caused by a size exclusion mechanism.

This behavior can be understood by considering the LbL assembly concept of intrinsic and extrinsic charge compensation.<sup>77–80</sup> The films present an excess of protonated

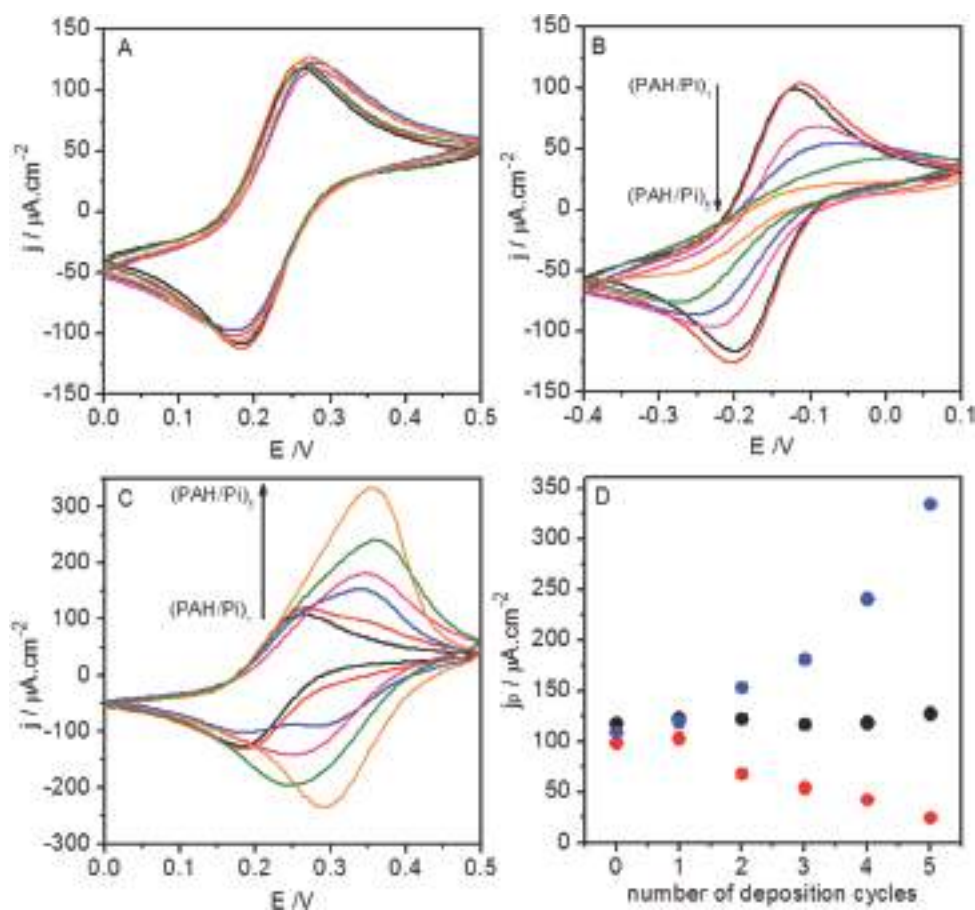


Fig. 9 Cyclic voltammograms of Au/cysteamine (black lines) and modified with PAH/Pi films formed from 0.2 mg mL<sup>-1</sup> PAH in 5 mM Pi pH 7, with a different number of deposition cycles: (PAH/Pi)<sub>1</sub> (red lines), (PAH/Pi)<sub>2</sub> (blue lines), (PAH/Pi)<sub>3</sub> (pink lines), (PAH/Pi)<sub>4</sub> (green lines) and (PAH/Pi)<sub>5</sub> (orange lines), in PBS buffer containing 1 mM of (A) FcOH, (B) Ru(NH<sub>3</sub>)<sub>6</sub><sup>3+</sup> and (C) Fe(CN)<sub>6</sub><sup>4-</sup>. (D) Peak anodic current density ( $j_p$ ) as a function of the number of deposition cycles for FcOH (black circles), Ru(NH<sub>3</sub>)<sub>6</sub><sup>3+</sup> (red circles) and Fe(CN)<sub>6</sub><sup>4-</sup> (blue circles). Error bars are smaller than the symbol size. Scan rate: 0.050 V s<sup>-1</sup>.

amines – that are not cross-linked by phosphate groups – in agreement with the positive zeta potential observed for the PAH/Pi solution phase complexes used in the surface assembly (Fig. 6B). This excess of amine groups is not intrinsically compensated by electrostatic interactions with phosphate ions in the film. Considering the electroneutrality requirement, they are compensated with mobile anions from the solution. Thus, the cationic probe must diffuse through a more positive environment observing a decrease in the permeation properties in a charge exclusion mechanism. This repulsion is more intense as the amount of the deposited material increases. As a consequence, the diffusion of  $\text{Ru}(\text{NH}_3)_6^{3+}$  is getting slower when the deposition cycles increase. In the case of the coating formed from  $0.05 \text{ mg mL}^{-1}$  PAH, all the protonated amine groups are intrinsically compensated, generating a more neutral surface environment that does not affect the diffusion of the ionic probe.

In the case of  $\text{Fe}(\text{CN})_6^{3-}$ , the electrochemical signal was stable and comparable with the unmodified electrode for all the assemblies, indicating that this anionic probe efficiently penetrates the PAH/Pi films (Fig. 9C). For  $(\text{PAH}/\text{Pi})_1$  a typical reversible cyclic voltammogram is obtained with a peak separation of 80 mV. However, for  $(\text{PAH}/\text{Pi})_2$ , a surface confined electron transfer process is detected by the appearance of a peak centered at 0.30–0.35 V with a minimum mass transport peak separation. This signal is produced by the confinement of the redox couple produced by the interaction of  $\text{Fe}(\text{CN})_6^{3-}$  with the positively charged amine groups of the PAH chains.<sup>81</sup> As the number of assembly steps increases, the surface confined signal becomes more relevant. At higher thickness values, the peaks were shifted in the positive direction and the peak current density increases significantly (Fig. 9D). To confirm the hypothesis, the electrode modified with PAH/Pi previously exposed to  $\text{Fe}(\text{CN})_6^{3-}$  solution was washed exhaustively. Then the CVs were recorded in a  $\text{Fe}(\text{CN})_6^{3-}$  ion-free buffer PBS (Fig. S5, ESI<sup>†</sup>). The peaks between 0.30 and 0.35 V corresponding to the electrochemical potentials of the confined species were observed, indicating that the films contain significant amounts of the redox probe. Moreover, it is also observed that the peak current decreases with the number of electrochemical cycles, suggesting that the  $\text{Fe}(\text{CN})_6^{3-}$  ions are released out of the films over time. A similar phenomenon was previously observed by Anzai *et al.* for multilayered polyelectrolyte films (PEM) generated by LbL assemblies where PAH was used as a building block.<sup>63,82</sup>

Taken altogether, the results allow us to infer that the PAH/Pi platforms present characteristics of hydrogels with a porous and highly hydrated polymer matrix. In addition, our architecture is completely integrated through non-covalent interactions, unlike other hydrogels reported with a modulable thickness. In addition, we note that it is possible to modulate transport properties within the supramolecular network with a simple variation of the polyelectrolyte concentration in the assembly process. Thus, the permeability of ionic species within the polymer matrix can rationally be tuned to build thin films completely permeable or with ion-transport selectivity.

## Conclusions

In this work, we further explored the bioinspired surface assembly of polyamines and phosphate anions, demonstrating that it is feasible to create entirely supramolecular nanoarchitectures with precise structural control, using a simple and reproducible strategy based on the continuous assembly of PAH/Pi networks. We have shown that the proposed protocol enables the formation of films with highly regular growth characteristics. Thus, this new “nanoarchitectonic approach” allows modulating the thickness of the coatings and the amount of the material deposited, not only with the self-assembly time and the concentration of the polycation but also with the assembly steps of PAH/Pi complexes.

In addition, these PAH/Pi films are pH-sensitive platforms showing entire disassembly behaviour in the presence of highly acidic or basic solutions. The transport properties of the interfacial coatings indicated that the supramolecular integrated PAH/Pi networks form a porous hydrogel matrix. Furthermore, the permeability within the polymer network can be simply modulated by varying the concentration of the polyelectrolyte in the assembly solution. Thus, ultrathin films with high permeability can be constructed from low bulk concentrations of PAH. However, the increase in the concentration of PAH in the assembly mixture leads to thicker films that present an excess of extrinsically compensated protonated amines, generating a membrane with high ionic permselectivity that inhibits the transport of cationic probes.

In summary, we consider that the possibility of continuously assembling the same building blocks through controllable and flexible processes – added to the interesting and tunable properties shown by the films – opens the opportunity to rationally explore the integration and combination of different functionalities for diverse technological applications.

## Conflicts of interest

There are no conflicts to declare.

## Acknowledgements

This work was supported by the Consejo Nacional de Investigaciones Científicas y Técnicas (CONICET, Argentina) (Grant No. PIP 0370), the Agencia Nacional de Promoción Científica y Tecnológica (ANPCyT, Argentina; PICT-2013-0905 and PICT-2016-1680), the Austrian Institute of Technology GmbH (the AIT-CONICET Partner Group: “*Exploratory Research for Advanced Technologies in Supramolecular Materials Science*”, Exp. 4947/11, Res. No. 3911, and 28-12-2011), and the Universidad Nacional de La Plata (UNLP) (PPID-X016). M. L. C., C. v. B., L. I. P., W. A. M. and O. A. are staff members of the CONICET. M. L. A. and S. E. H. gratefully acknowledge the CONICET for their postdoctoral fellowships.

## References

- 1 K. Ariga, M. V. Lee, T. Mori, X.-Y. Yu and J. P. Hill, *Adv. Colloid Interface Sci.*, 2010, **154**, 20–29.

- 2 M. Aono, Y. Bando and K. Ariga, *Adv. Mater.*, 2012, **24**, 150–151.
- 3 M. Ramanathan, L. K. Shrestha, T. Mori, Q. Ji, J. P. Hill and K. Ariga, *Phys. Chem. Chem. Phys.*, 2013, **15**, 10580–10611.
- 4 (a) K. Ariga, V. Malgras, Q. Ji, M. B. Zakaria and Y. Yamauchi, *Coord. Chem. Rev.*, 2016, **320–321**, 139–152; (b) K. Ariga, M. Nishikawa, T. Mori, J. Takeya, L. K. Shrestha and J. P. Hill, *Sci. Technol. Adv. Mater.*, 2018, DOI: 10.1080/14686996.2018.1553108.
- 5 (a) A. H. Khan, S. Ghosh, B. Pradhan, A. Dalui, L. K. Shrestha, S. Acharya and K. Ariga, *Bull. Chem. Soc. Jpn.*, 2017, **90**, 627–648; (b) M. Komiyama, T. Mori and K. Ariga, *Bull. Chem. Soc. Jpn.*, 2018, **91**, 1075–1111.
- 6 (a) K. Ariga, Y. Yamauchi, G. Rydzek, Q. Ji, Y. Yonamine, K. C.-W. Wu and J. P. Hill, *Chem. Lett.*, 2014, **43**, 36–68; (b) M. Komiyama, K. Yoshimoto, M. Sisido and K. Ariga, *Bull. Chem. Soc. Jpn.*, 2017, **90**, 967–1004.
- 7 K. Ariga, A. Vinu, Y. Yamauchi, Q. Ji and J. P. Hill, *Bull. Chem. Soc. Jpn.*, 2012, **85**, 1–32.
- 8 G. Decher, J.-D. Hong and B. Bunsenges, *Phys. Chem.*, 1991, **95**, 1430–1434.
- 9 G. Decher, *Science*, 1997, **277**, 1232–1237.
- 10 M. L. Cortez, N. De Matteis, M. Ceolin, W. Knoll, F. Battaglini and O. Azzaroni, *Phys. Chem. Chem. Phys.*, 2014, **16**, 20844–20855.
- 11 O. Azzaroni and K. H. A. Lau, *Soft Matter*, 2011, **7**, 8709–8724.
- 12 M. Ali, B. Yameen, J. Cervera, P. Ramirez, R. Neumann, W. Ensinger, W. Knoll and O. Azzaroni, *J. Am. Chem. Soc.*, 2010, **132**, 8338–8348.
- 13 J. Irigoyen, S. E. Moya, J. J. Iturri, I. Llarena, O. Azzaroni and E. Donath, *Langmuir*, 2009, **25**, 3374–3380.
- 14 H. Lee, S. M. Dellatore, W. M. Miller and P. B. Messersmith, *Science*, 2007, **318**, 426–430.
- 15 H. Lee, Y. Lee, A. R. Statz, J. Rho, T. G. Park and P. B. Messersmith, *Adv. Mater.*, 2008, **20**, 1619–1623.
- 16 S. M. Kang, N. S. Hwang, J. Yeom, S. Y. Park, P. B. Messersmith, I. S. Choi, R. Langer, D. G. Anderson and H. Lee, *Adv. Funct. Mater.*, 2012, **22**, 2949–2955.
- 17 W. A. Marmisollé, J. Irigoyen, D. Gregurec, S. Moya and O. Azzaroni, *Adv. Funct. Mater.*, 2015, **25**, 4144–4152.
- 18 N. E. Muzzio, M. A. Pasquale, W. A. Marmisollé, C. von Bilderling, M. L. Cortez, L. I. Pietrasanta and O. Azzaroni, *Biomater. Sci.*, 2018, **6**, 2230–2247.
- 19 L. D'Agostino and A. Di Luccia, *Eur. J. Biochem.*, 2002, **269**, 4317–4325.
- 20 N. Kroger, R. Deutzman, C. Bergsdorf and M. Sumper, *Proc. Natl. Acad. Sci. U. S. A.*, 2000, **97**, 14133–14138.
- 21 A. Di Luccia, G. Picariello, G. Iacomino, A. Formisano, L. Paduano and L. D'Agostino, *FEBS J.*, 2009, **276**, 2324–2335.
- 22 M. Sumper, *Angew. Chem., Int. Ed.*, 2004, **43**, 2251–2254.
- 23 M. Sumper and N. Kroger, *J. Mater. Chem.*, 2004, **14**, 2059–2065.
- 24 G. Iacomino, G. Picariello, F. Sbrana, A. Di Luccia, R. Raiteri and L. D'Agostino, *Biomacromolecules*, 2011, **12**, 1178–1186.
- 25 E. Brunner, K. Lutz and M. Sumper, *Phys. Chem. Chem. Phys.*, 2004, **6**, 854–857.
- 26 M. Sumper, S. Lorenz and E. Brunner, *Angew. Chem., Int. Ed.*, 2003, **42**, 5192–5195.
- 27 M. Mouslmani, J. M. Rosenholm, N. Prabhakar, M. Peurla, E. Baydoun and D. Patra, *RSC Adv.*, 2015, **5**, 18740–18750.
- 28 L. D'Agostino, M. di Pietro and A. Di Luccia, *FEBS J.*, 2005, **272**, 3777–3787.
- 29 K. Lutz, C. Groger, M. Sumper and E. Brunner, *Phys. Chem. Chem. Phys.*, 2005, **7**, 2812–2815.
- 30 E. Hubsch, V. Ball, B. Senger, G. Decher, J. C. Voegel and P. Schaaf, *Langmuir*, 2004, **20**, 1980–1985.
- 31 V. Kozlovskaya, E. Kharlampieva, M. L. Mansfield and S. A. Sukhishvili, *Chem. Mater.*, 2006, **18**, 328–336.
- 32 J. J. Richardson, B. L. Tardy, H. Ejima, J. Guo, J. Cui, K. Liang, G. H. Choi, P. J. Yoo, B. G. De Geest and F. Caruso, *ACS Appl. Mater. Interfaces*, 2016, **8**, 7449–7455; S. R. Bhatia, S. F. Khatkhat and S. C. Roberts, *Curr. Opin. Colloid Interface Sci.*, 2005, **10**, 45–51.
- 33 E. Kharlampieva, V. Kozlovskaya and S. A. Sukhishvili, *Adv. Mater.*, 2009, **21**, 3053–3065.
- 34 E. Kharlampieva, I. Erel-Unal and S. A. Sukhishvili, *Langmuir*, 2007, **23**, 175–181.
- 35 Y. Fu, S. Bai, S. Cui, D. Qiu, Z. Wang and X. Zhang, *Macromolecules*, 2002, **35**, 9451–9458.
- 36 V. A. Kozlovskaya, E. P. Kharlampiev, I. Erel-Unal and S. A. Sukhishvili, *Polym. Sci., Ser. A*, 2009, **51**, 719–729.
- 37 E. S. Dragan and F. Bucatariu, *Macromol. Rapid Commun.*, 2010, **31**, 317–322.
- 38 V. A. Kozlovskaya, E. P. Kharlampieva, I. Erel-Unal and S. A. Sukhishvili, *Polym. Sci., Ser. A*, 2009, **51**, 719–729.
- 39 Y. Zhang, Y. Guan and S. Zhou, *Biomacromolecules*, 2005, **6**, 2365–2369.
- 40 Z. Wang, H. Zhu, D. Li and X. Yang, *Colloids Surf., A*, 2008, **329**, 58–66.
- 41 F. Bucatariu, G. Fundueanu, G. Hitruc and E. S. Dragan, *Colloids Surf., A*, 2011, **380**, 111–118.
- 42 U. Manna, J. Dhar, R. Nayak and S. Patil, *Chem. Commun.*, 2010, **46**, 2250–2252.
- 43 G. K. Such, J. F. Quinn, A. Quinn, E. Tjpto and F. Caruso, *J. Am. Chem. Soc.*, 2006, **128**, 9318–9319.
- 44 W. Tong, C. Gao and H. Möhwald, *Macromol. Rapid Commun.*, 2006, **27**, 2078–2083.
- 45 L. D'Agostino, M. di Pietro and A. Di Luccia, *FEBS J.*, 2005, **272**, 3777–3787.
- 46 (a) E. E. Kooijman, D. P. Tieleman, C. Testerink, T. Munnik, D. T. S. Rijkers, K. N. J. Burger and B. De Kruijff, *J. Biol. Chem.*, 2007, **282**, 11356–11364; (b) E. E. Kooijman and K. N. J. Burger, *Biochim. Biophys. Acta, Mol. Cell Biol. Lipids*, 2009, **1791**, 881–888.
- 47 (a) D. A. Capdevila, W. A. Marmisollé, F. J. Williams and D. H. Murgida, *Phys. Chem. Chem. Phys.*, 2013, **15**, 5386–5394; (b) W. A. Marmisolle, D. A. Capdevila, E. De Llave, F. J. Williams and D. H. Murgida, *Langmuir*, 2013, **29**, 5351–5359.
- 48 W. A. Marmisollé, J. Irigoyen, D. Gregurec, S. Moya and O. Azzaroni, *Adv. Funct. Mater.*, 2015, **25**, 4144–4152.
- 49 K. Lutz, C. Gröger, M. Sumper and E. Brunner, *Phys. Chem. Chem. Phys.*, 2005, **7**, 2812–2815.

- 50 W. J. Dressick, K. J. Wahl, N. D. Bassim, R. M. Stroud and D. Y. Petrovykh, *Langmuir*, 2012, **28**, 15831–15843.
- 51 G. Laucirica, W. A. Marmisollé and O. Azzaroni, *Phys. Chem. Chem. Phys.*, 2017, **19**, 8612–8620.
- 52 (a) C. Sun and D. Xue, *J. Mol. Struct.*, 2014, **1059**, 338–342; (b) C. Sun and D. Xue, *J. Phys. Chem. C*, 2014, **118**, 16043–16050.
- 53 M. Eriksson, S. M. Notley and L. Wågberg, *J. Colloid Interface Sci.*, 2005, **292**, 38–45.
- 54 P. Andreozzi, E. Diamanti, K. R. Py-Daniel, P. R. Cáceres-Vélez, C. Martinelli, N. Politakos, A. Escobar, M. Muzi-Falconi, R. Azevedo and S. E. Moya, *ACS Appl. Mater. Interfaces*, 2017, **9**, 38242–38254.
- 55 V. S. Murthy, R. K. Rana and M. S. Wong, *J. Phys. Chem. B*, 2006, **110**, 25619–25627.
- 56 Y. Xia, T. D. Nguyen, M. Yang, B. Lee, A. Santos, P. Podsiadlo, Z. Tang, S. C. Glotzer and N. Kotov, *Nat. Nanotechnol.*, 2011, **6**, 580–587.
- 57 S. Pavlukhina and S. Sukhishvili, *Adv. Drug Delivery Rev.*, 2012, **63**, 822–836.
- 58 S. R. Bhatia, S. F. Khatkhat and S. C. Roberts, *Curr. Opin. Colloid Interface Sci.*, 2005, **10**, 45–51.
- 59 X. Z. Shu and K. J. Zhu, *Eur. J. Pharm. Biopharm.*, 2002, **54**, 235–243.
- 60 Y. Huang, P. G. Lawrence and Y. Lapitsky, *Langmuir*, 2014, **26**, 7771–7777.
- 61 P. G. Lawrence and Y. Lapitsky, *Langmuir*, 2015, **31**, 1564–1574.
- 62 J. J. Keating, J. Imbrogno and G. Belfort, *ACS Appl. Mater. Interfaces*, 2016, **8**, 28383–28399.
- 63 X. Liu and M. L. Bruening, *Chem. Mater.*, 2004, **16**, 351–357.
- 64 M. L. Cortez, W. Marmisollé, D. Pallarola, L. I. Pietrasanta, D. H. Murgida, M. Ceolín, O. Azzaroni and F. Battaglini, *Chem. – Eur. J.*, 2014, **20**, 13366–13374.
- 65 R. M. Flessner, Y. Yu and D. M. Lynn, *Chem. Commun.*, 2011, **47**, 550–552.
- 66 E. Vazquez, D. M. Dewitt, P. T. Hammond and D. M. Lynn, *J. Am. Chem. Soc.*, 2002, **124**, 13992–13993.
- 67 L. Han, X. Lu, K. Liu, K. Wang, L. Fang, L.-T. Weng, H. Zhang, Y. Tang, F. Ren, C. Zhao, G. Sun, R. Liang and Z. Li, *ACS Nano*, 2017, **11**, 2561–2574.
- 68 L. Krasemann, A. Toutianoush and B. Tieke, *J. Membr. Sci.*, 2001, **181**, 221–228.
- 69 A. M. Balachandra, J. H. Dai and M. L. Bruening, *Macromolecules*, 2002, **35**, 3171–3178.
- 70 R. Takita, Y. Okamura, Y. Endo and J. I. Anzai, *Electroanalysis*, 2006, **18**, 1627–1630.
- 71 T. Noguchi and J. I. Anzai, *Langmuir*, 2006, **22**, 2870–2875.
- 72 S. E. Burke and C. J. Barrett, *Macromolecules*, 2004, **37**, 5375–5384.
- 73 M. K. Park, S. Deng and R. C. Advincula, *J. Am. Chem. Soc.*, 2004, **126**, 13723–13731.
- 74 J. Dai, A. M. Balachandra, J. I. Lee and M. L. Bruening, *Macromolecules*, 2002, **35**, 3164–3178.
- 75 Q. Li, J. F. Quinn and F. Caruso, *Adv. Mater.*, 2005, **17**, 2058–2062.
- 76 J. L. Zhang, M. E. Williams, M. H. Keefe, G. A. Morris, S. T. Nguyen and J. T. Hupp, *Electrochem. Solid-State Lett.*, 2002, **5**, 25–28.
- 77 J. B. Schlenoff, H. Ly and M. Li, *J. Am. Chem. Soc.*, 1998, **120**, 7626–7634.
- 78 L. Krasemann and B. Tieke, *Langmuir*, 2000, **16**, 287–290.
- 79 T. R. Farhat and J. B. Schlenoff, *Langmuir*, 2001, **17**, 1184–1192.
- 80 T. R. Farhat and J. B. Schlenoff, *J. Am. Chem. Soc.*, 2003, **125**, 4627–4636.
- 81 M. Villalba, L. P. Méndez De Leo and E. J. Calvo, *ChemElectroChem*, 2014, **1**, 195–199.
- 82 R. Takita, K. Yoshida and J. I. Anzai, *Sens. Actuators, B*, 2007, **121**, 54–60.